
Article:
Blain, T. orcid.org/0000-0002-7974-7355, Shulyak, V. orcid.org/0000-0001-5223-0930, Han, I.S. et al. (3 more authors) (2024) Low noise equivalent power InAs avalanche photodiodes for infrared few-photon detection. IEEE Transactions on Electron Devices. ISSN 0018-9383

https://doi.org/10.1109/ted.2024.3373373

Low Noise Equivalent Power InAs Avalanche Photodiodes for Infrared Few-Photon Detection

Tarick Blain, Vladimir Shulyak, Im Sik Han, Mark Hopkinson, Jo Shien Ng, *Member, IEEE,* and Chee Hing Tan, *Senior Member, IEEE*

***Abstract*—Electron-only avalanche multiplication and low excess noise has previously been established in InAs avalanche photodiodes. However, there is currently a lack of experimental investigations into the noise and low photon detection capability of planar InAs avalanche photodiodes. Here, the noise equivalent power of planar InAs avalanche photodiodes operating with a low noise transimpedance amplifier is investigated for the first time. Our devices have responsivity of 0.7 A/W and excellent linearity at the wavelength of 1550 nm. Using these avalanche photodiodes, a very low noise equivalent power of 45 fW/$\sqrt{\text{Hz}}$ is achieved at a gain of 54. Modeling of the NEP suggests the excess factor is close to 1.6. This low NEP result is corroborated by detection of weak optical pulses corresponding to <70 photons per 1550 nm laser pulse. Our analysis suggests that this performance can be enhanced through suppression of the background component of the photocurrent as well as reducing the unintentional doping in the devices.**

***Index Terms*—Avalanche Photodiodes (APDs), Infrared detectors, InAs, Noise equivalent power.**

I. INTRODUCTION

Detection of weak photon fluxes in the short-wave infrared (SWIR) is important for a wide variety of commercial and scientific applications. These include fiber optic communication systems [1], light detection and ranging (LIDAR) [2], and remote gas sensing [3]. Avalanche photodiodes (APDs) are a popular detector choice in many of these applications, owing to the enhanced signal-to-noise ratio (SNR) of the receiver circuit afforded by the APD's internal avalanche gain. A common figure of merit for APD-based receiver is noise equivalent power (NEP), defined as the minimum optical power per unit bandwidth required to produce SNR = 1. To achieve a low NEP, the receiver circuit requires (i) a low noise transimpedance amplifier, and (ii) an APD exhibiting high avalanche gain (M), high external quantum efficiency (η), low dark current and low excess noise factor (F). The excess noise of an APD results from the stochastic nature of the avalanche multiplication process. To achieve low excess noise, materials with highly disparate electron and hole ionization coefficients (α and β respectively) should be used for multiplication. Hence, the ratio of these coefficients ($k = \beta/\alpha$) is a convenient figure of merit for comparing excess noise performance of different APDs. The excess noise factor of an APD can be estimated using the ionization coefficient ratio and McIntyre's local model [4] given as

$$F = kM + (1-k)\left(2 - \frac{1}{M}\right). \quad (1)$$

APDs with low k therefore exhibit the lowest excess noise factors. For the special case of $k = 0$, F asymptotically approaches 2 with increasing M.

Commercial APDs operating at ~ 1550 nm wavelengths are dominated by separate-absorption-multiplication (SAM) structures that combine InGaAs absorbers with InP multipliers. Typical excess noise performance of InGaAs/InP SAM APDs is F ~ 3.5 at M ~ 10 [5]. They are widely available and hybridized detector/amplifier assemblies offer NEPs as low as 130 fW/$\sqrt{\text{Hz}}$ at 1550 nm [6]. More recently, SAM APDs utilizing AlGaAsSb multipliers with InGaAs or GaAsSb absorbers for 1550 nm wavelength operation have demonstrated very high gains with low excess noise factors [7] leading to NEPs as low as 69 fW/$\sqrt{\text{Hz}}$ when operating with a transimpedance amplifier [8].

Materials with k = 0 and therefore the lowest excess noise factors include InSb, HgCdTe and InAs. Their bandgaps are much narrower than that of InP, so cooling is required to achieve optimum performance. Reliable avalanche gain in InSb is limited to 3 due to significant tunneling currents [9]. Liquid nitrogen cooled HgCdTe APDs have good performance, achieving M > 600 with F ~ 1 [10]. Hybridized HgCdTe APD/amplifier assemblies exhibit NEPs below 0.5 fW/$\sqrt{\text{Hz}}$ at 1550 nm wavelength, enabling linear mode photon counting [11]. There are however challenges preventing wider spread adoption of this technology: cost, growth and fabrication complexity [12] as well as an initiative to reduce use of Hg in new products [13].

Experimental reports of InAs APDs have established that $F \approx 1.6$ largely independent of gain and temperature [14]. Mesa InAs APDs can therefore detect very weak optical signals down to 15-31 photons per 50 µs pulse at 1550 nm wavelength [15]. InAs APDs with both mesa [16] and planar [17] topologies exhibited M > 100. Bandwidths up to 3.5 GHz were reported without a gain-bandwidth product limit (owing to k = 0) [18]. Recent InAs APD reports utilized planar topology to reduce surface-related leakage current [19].

Manuscript received 25 January 2024; revised 27 February 2024; accepted 28 February 2024. This work was supported by the U.K.-Engineering and Physical Sciences Research Council under Grant EP/S026428/1. (Corresponding author: Chee Hing Tan.)

Tarick Blain, Im Sik Han, Mark Hopkinson, Jo Shien Ng and Chee Hing Tan are with the Department of Electronic and Electric Engineering, The University of Sheffield, Sheffield S13JD, U.K. (e-mail: t.blain@sheffield.ac.uk; i.han@sheffield.ac.uk; m.hopkinson@sheffield.ac.uk; j.s.ng@sheffield.ac.uk; c.h.tan@sheffield.ac.uk).

Vladimir Shulyak was previously the Department of Electronic and Electric Engineering, The University of Sheffield and is now with Connector Subsea Solutions, Wednesbury, WS10 8LX, UK. (e-mail: research@shulyak.co.uk).

Color versions of one or more of the figures in this article are available online at http://ieeexplore.ieee.org

Although current HgCdTe APDs exhibit superior performance, InAs APDs offer several advantages: wafer growth requires standard III-V growth chambers from a number of widely accessible foundries; less complex growth (as a binary alloy) and lower cost native substrates are widely available.

Ref [16] reported low photon detection capability of InAs APDs operated at low temperatures, but it used APDs with mesa topology and no NEP data was reported. Therefore, in this paper we report an experimental NEP study on planar InAs APDs operating with a low noise transimpedance amplifier at 1550 nm wavelength.

II. Experimental Details

InAs epilayers were grown by molecular beam epitaxy on 2" (100) vertical temperature gradient freezing substrates. The epilayers consisted of 600 nm of Si doped n-InAs followed by 9.6 µm of unintentionally doped InAs. The layers were grown at a substrate temperature of 480 °C at a rate of 3 Å/s. The growth conditions were optimized to produce intrinsic InAs layers with minimal unintentional doping. This helps to achieve the wide depletion widths, maximizing the APD's avalanche gain. Wafers grown at temperatures lower than 480 °C exhibited higher levels of unintentional doping whereas those grown at higher temperatures exhibited higher defect levels and rougher surface morphology.

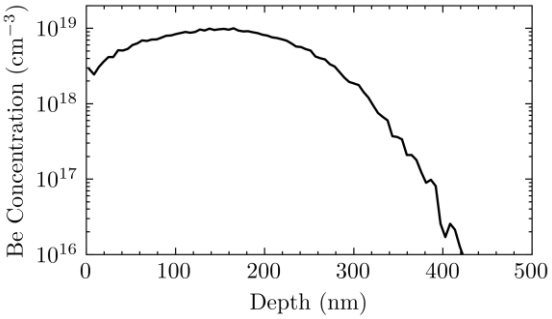

Fig. 1. Simulated Be implant profile produced using Transport of Ions in Matter software [20].

Planar InAs APDs with remote bondpads were fabricated using a similar method to [19]. Device fabrication started with defining the p^+ regions on the InAs sample using photoresist. The p^+ regions were formed using beryllium (Be) ion implantation with an energy of 45 keV and a dose of 2.3×10^{14} cm^{-2}. The conditions were chosen to produce a Be implant profile with a projected range of ~200 nm, based on simulation results shown in Fig. 1 [20]. After ion implantation, the sample was annealed at 550 °C for 30 s. A cross-sectional diagram of the device structure is shown in Fig. 2 (top) along with a scanning electron microscope image of several 80×80 µm^2 pixels (bottom). Device fabrication also produced devices without remote bondpads and they were reserved for capacitance measurements to extract doping profiles. Since the Be implanted p^+ region is shallow, only ~ 42% of the 1550 nm wavelength illumination would be absorbed in the p^+ region, with the rest of the illumination resulting in a mixture of electrons and holes within the InAs avalanche region.

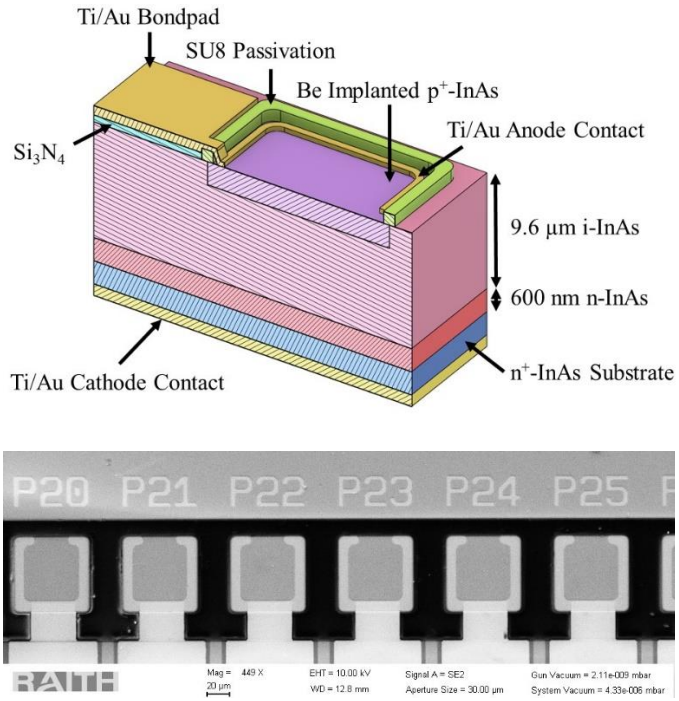

Fig. 2. Cross-sectional diagram of planar InAs APD device structure (not drawn to scale) (top). Scanning electron microscope image of several 80×80 µm^2 pixels (bottom).

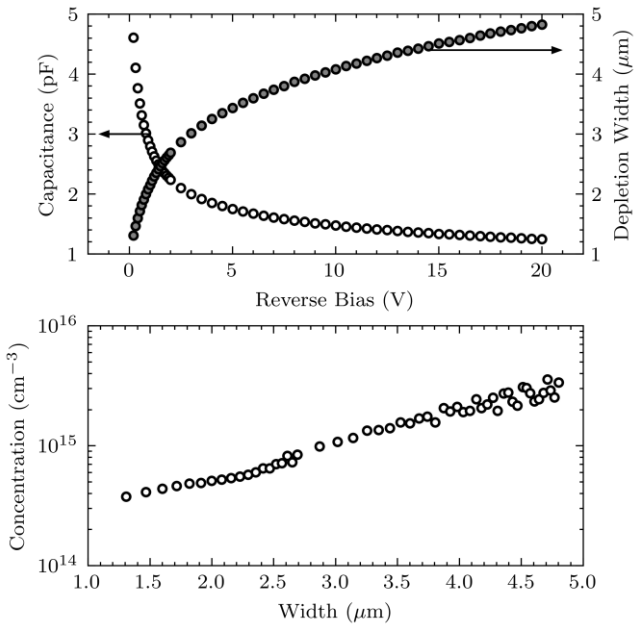

Fig. 3. Capacitance (open symbols) and depletion width (closed symbols) of a 200×200 µm^2 pixel (top) and unintentional doping level extracted from the capacitance measurement (bottom).

Capacitance-voltage measurements at 77 K were performed on the APDs without bondpads with active areas of 400×400, 200×200 and 100×100 µm^2 in a low-temperature

probe station connected to a LCR meter. The depletion width and unintentional doping level extracted from capacitance-voltage measurements are presented in Fig. 3. At -20 V, the depletion width is less than 5 µm, which is just over half of the nominal intrinsic width. The unintentional doping is n-type, which had been established from measurements on p-i-n and n-i-p mesa diodes grown under similar conditions [21]. The unintentional doping level was found to be very low closer to the p-i interface, however, reaches excessive levels deeper into the structure.

Separate temperature dependent dark current measurements were carried out on APDs with the same active areas packaged into TO-5 headers, which were placed in a helium-cooled cryostat. During the dark current measurements, the APDs were covered by a cooled solid metal cap to avoid the dark current data being affected by blackbody radiation.

NEP and low light level measurements were performed on 80×80 µm^2 APDs packaged into TO-5 headers. The headers were placed in a liquid nitrogen dewar, which cooled the APDs to 135-140 K (due to imperfect temperature coupling between the cold finger and the TO-5 socket). The APD's photocurrent was fed to a low noise transimpedance amplifier (model SR570). The voltage output of the amplifier was connected to a Fast Fourier Transform (FFT) spectrum analyzer (model SR760). The gain and responsivity were measured under illumination of a 1550 nm 10 kHz modulated laser using a lock-in amplifier and were also verified by measuring the signal peaks on the FFT spectrum analyzer. The optical power incident upon the detectors from the 1550 nm laser was controlled using a calibrated electronic variable attenuator (model EXFO FVA-3100) capable of up to 60 dB attenuation with a linearity of ±0.1 dB.

The NEP was taken as the mean noise floor measured on the FFT spectrum analyzer around 10 kHz (with 100 Hz span) in A/$\sqrt{\text{Hz}}$ divided by the APDs bias dependent responsivity curve. This frequency was chosen as it was above any 1/f noise and within the spectrum analyzers bandwidth of 100 kHz. The sensitivity of the pre-amplifier was set to 10^{-5} A/V and the input referred current noise spectral density (n_{amp}) was ~1 pA/$\sqrt{\text{Hz}}$. Using these settings, the amplifiers bandwidth was 200 kHz. SNR measurements were derived from the FFT spectra with the devices under illumination. The signal peak was measured at 10 kHz while the noise was taken as the mean value of the adjacent frequency bins.

III. Results and Discussion

Reverse dark current and the gain resulting from 1550 nm wavelength illumination of an 80×80 µm^2 InAs APD at 135-140 K is shown in Fig. 4. Gain as high as 105 was obtained. The unmultiplied dark current, estimated by dividing the raw dark current data with the gain data, is also plotted. The increase in gain normalized dark current at bias > 20 V is attributed to non-avalanche mechanism, believed to be band to band tunneling. The maximum achievable avalanche gain here is lower than previously reported planar InAs APD, which reached gains of 330 with a gain normalized dark current density of 400 µA cm^{-2} at 200 K measured on 200 µm diameter circular pixels [17]. The detectors presented here with a similar active area (200×200 µm^2) to those in [17] exhibited a gain normalized dark current density of 700 µA cm^{-2} at the same temperature.

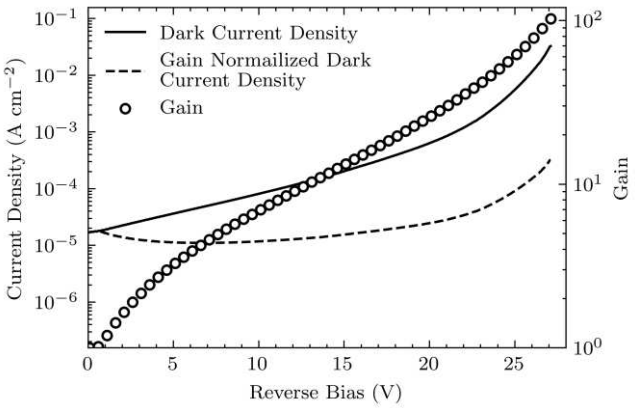

Fig. 4. Reverse dark current density (solid line), avalanche gain (symbols) and gain normalized dark current density (dashed line) of a packaged 80×80 µm^2 pixel measured in a liquid nitrogen cooled cryostat.

The NEP curve in Fig. 5 was derived from the responsivity and noise measurements centered around 10 kHz (100 Hz span) using an FFT spectrum analyzer. The unity gain responsivity of these detectors was found to be 0.7 A/W, corresponding to an η of 56 %, which is a 5 % improvement compared to the current best reported value for planar InAs of 0.62 A/W [22]. A very low NEP of 45 fW/$\sqrt{\text{Hz}}$ occurs at a gain of 54. The increase in NEP at higher gains can be attributed to the dominance of tunneling current at higher biases (modeling of the NEP and dark current analysis are presented in the later part of this section).

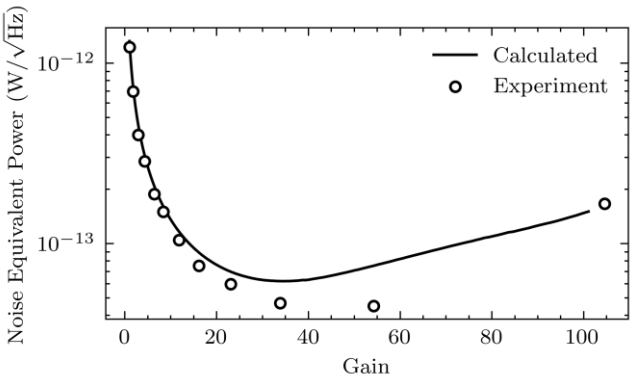

Fig. 5. 1550 nm wavelength noise equivalent power of the APD/preamp configuration measured around 10 kHz with a 100 Hz span (symbols) and theoretical NEP calculated from Eq. 2 (solid line).

To further corroborate the measured high gain and low NEP, SNR and weak light level measurements were also performed. The SNR data are presented in Fig. 6 (top). An average signal power of 8.77 pW at a modulation frequency of 10 kHz was chosen as this level brought the signal peak above the amplifier dominated noise floor while the detector was biased at its unity gain point. Fig. 6 (bottom) shows the measured spectra at three points, with the detector biased around its unity gain point, at the maximum SNR (M = 54), and the maximum gain (M = 105). An M = 54 provides an SNR enhancement of 28.4 dB.

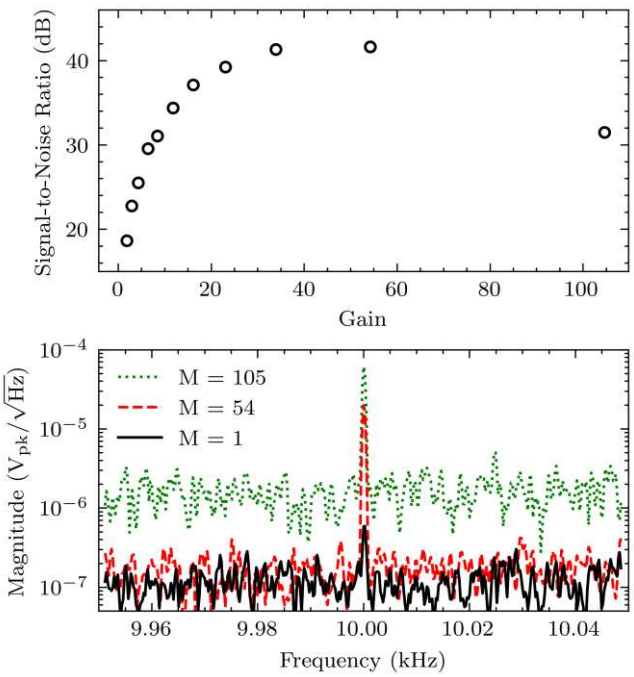

Fig. 6. Signal-to-noise ratio measurement (top) on a cooled 80×80 µm^2 pixel illuminated with a 1550 nm laser modulated at 10 kHz with an average optical power of 8.77 pW. Measured FFT spectra (bottom) at avalanche gains of 1 (solid black line), 54 (dashed red line), and 105 (dotted green line).

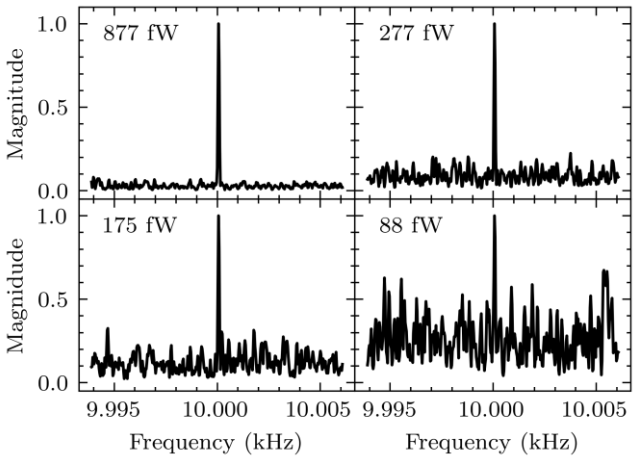

Fig. 7. FFT spectra around 10 kHz (12 Hz span) with the detectors illuminated with weak 10 kHz modulated 1550 nm wavelength pulses.

Since the APD/transimpedance amplifier configuration exhibited an NEP minimum and SNR maximum around an APD gain of 54, the APDs were biased to this gain and the optical power was attenuated using a calibrated electronic variable attenuator. The normalized FFT spectra for optical powers down to 88 fW (corresponding to < 70 photons per 50 µs pulse) are shown in Fig. 7. The linearity of the signal peak is presented in Fig. 8. At these low optical powers, the detector exhibits excellent linearity with a coefficient of determination of 0.9998, demonstrating the ability to resolve optical pulses corresponding to low photon numbers.

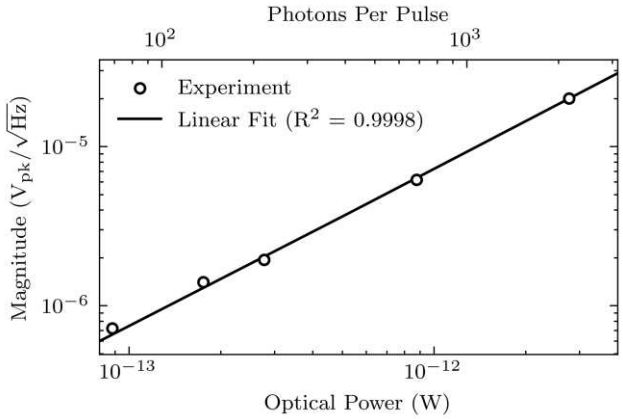

Fig. 8. Magnitudes of signal peaks at low optical powers (symbols) and linear fit (solid line).

Having established that the detectors are capable of providing very low NEP, large SNR enhancement, and detecting very low photon levels, our attention is turned to further device and set-up level optimizations. The input referred current noise spectral density of the transimpedance amplifier is lower than most transimpedance amplifiers currently on the market. Hence, there is limited scope for further improvements in this regard. To achieve even lower NEP, the detectors dark current needs to be reduced and its gain/responsivity increased. Since InAs exhibits a cut-off wavelength between 3 and 3.5 µm between 77 and 300 K, black-body radiation emanating from room temperature objects will have an adverse effect on the noise level of the detectors, especially at low temperatures when the dark current is low. The optical measurements were performed without the use of a cold shield and the kBr optical window was not cooled with the detectors, hence, the measured current under dark conditions was found to be dominated by black-body radiation. This effect is illustrated in Fig. 9 which compares the measured forward and reverse current of 80×80 µm^2 and 200×200 µm^2 pixels both with and without a cooled metal cap on the TO-5 package. The presence of black-body radiation is evidenced by the open circuit voltage on the current-voltage curve of the un-shielded detector. The un-multiplied reverse current increases by over one order of magnitude without any shielding from black-body radiation. Hence, the NEP could be reduced further through the use of cooled optical band-pass filters or by fiber coupling the detectors through a cold-shield.

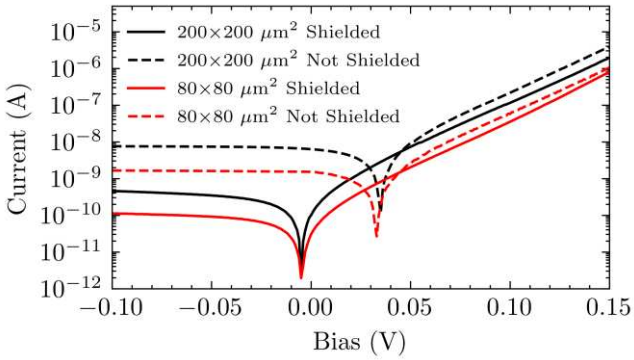

Fig. 9. Comparison of current-voltage characteristics of 80×80 μm^2 (red lines) and a 200×200 μm^2 (black lines) pixels with (solid lines) and without (dashed lines) shielding from black body radiation.

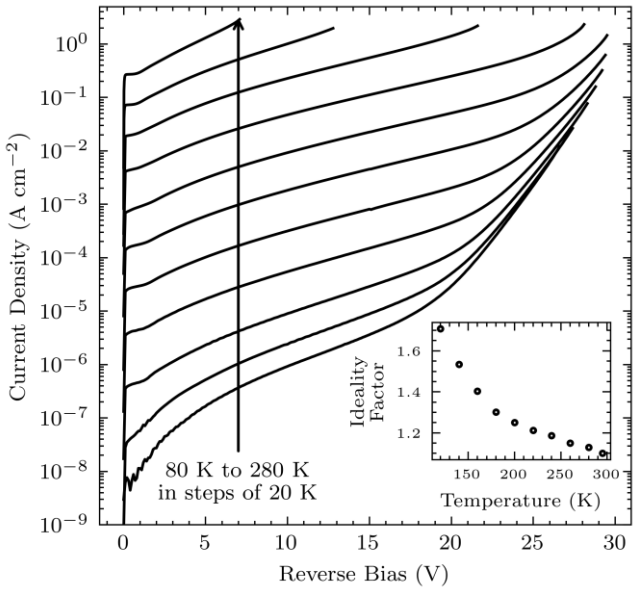

Fig. 10. Reverse dark current density temperature dependence of a shielded 200×200 μm^2 pixel between 80 and 280 K. The inset shows the temperature dependence of the diode's ideality factor extracted from the forward current-voltage data of Fig. 9.

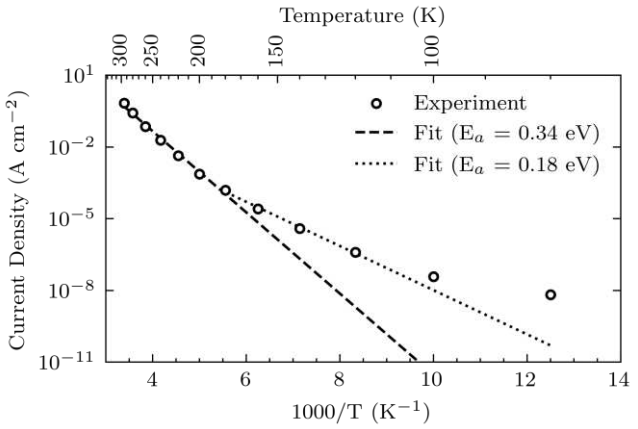

Fig. 11. Temperature dependence of the dark current density at -0.1 V for a 200×200 μm^2 pixel (symbols) and Arrhenius fits between 295 and 180 K (dashed line) and 180 to 120 K (dotted line).

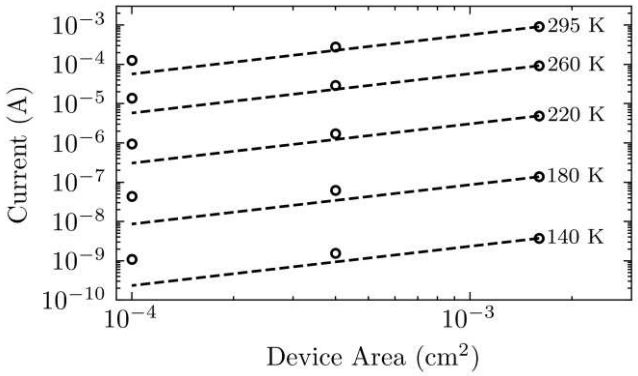

Fig. 12. Dark currents at -0.1 V of pixels of different areas measured between 295 K and 140 K (symbols) plotted with expected bulk dark currents extrapolated from the largest area pixels (dashed lines).

Further analysis of the dark current was performed on shielded devices. The temperature dependence of the reverse dark current of a 200×200 μm^2 pixel is shown in Fig. 10. Between 280 and 80 K a >7 order of magnitude reduction in the reverse dark current is observed. The observed convergence of the temperature dependent dark current after ~22.5 V reverse bias is indicative of excessive tunneling currents. Diode ideality factors extracted from the forward current increased gradually from ~1.1 to 1.3 between 280 and 180 K and increased rapidly towards 2 with decreasing temperature below 180 K. Hence, the forward current is diffusion dominated down to 180 K while generation-recombination (GR) mechanisms begin to dominate for temperatures below 180 K. Arrhenius plots of the dark current with the detectors biased around their unity gain points are presented for 200×200 μm^2 in Fig. 11. Down to 180 K, the extracted activation energy is roughly the bandgap of InAs. Hence, in this temperature range the dark current is diffusion dominated. Between 180 and 120 K the extracted activation energy is around half of the InAs bandgap. Below 120 K the activation energy continues to decrease. An increased dark current density was also observed on the smaller sized pixels as the detectors were cooled, as shown in Fig. 12. Hence, it is likely that surface and GR components are limiting the dark current at lower temperatures. Further optimizations to growth conditions (e.g. growing at higher temperature) and passivation techniques (e.g. performing overgrowth of lattice matched wide bandgap material) will be required to suppress these components.

To understand the effects of dark current, excess noise factor, and amplifier noise on the NEP, we attempted to model the NEP in Fig. 5 using

$$NEP = \frac{\sqrt{2qM^2F\langle I_{dp}\rangle + n_{amp}^2}}{\eta M \frac{q\lambda}{hc}}, \quad (2)$$

where q is the elementary charge, I_{dp} is the APD primary dark current (which is assumed to be the gain normalized dark current), n_{amp} is the amplifiers input referred current noise spectral density in $\mathrm{A}/\sqrt{\mathrm{Hz}}$, η is the experimental APD quantum efficiency, λ is the wavelength of operation, h is Planck's constant and c is the speed of light. We found that F = 1.6 produces a reasonably good fit. The slight discrepancy between the modelled and measured NEP curves in Fig. 5 can be explained by the presence of dark current mechanisms other than diffusion. Eq. 2 assumes that the dark current (I_d) scales with avalanche gain (i.e. $I_d = MI_{dp}$). This is a valid assumption only when the dark current is dominated by diffusion of electrons from the p$^+$ region. If the dark current is dominated by other mechanisms where carriers are generated outside of the p$^+$ region (such as tunneling or GR), then it will be subjected to different values of M and F, which explains the discrepancy in Fig. 5.

The NEP is ultimately limited by tunneling current at the highest possible gains. Suppression of this component can be achieved by maximizing the detectors depletion width, which requires low unintentional doping levels. This will also increase the avalanche gain of the detectors resulting in an overall reduction in NEP.

IV. Conclusion

InAs based APDs are capable of achieving very low NEPs due to their very low excess noise. A low 1550 nm NEP of 45 fW/Hz was demonstrated, despite moderate levels of mixed injection and background radiation. This low NEP can be attributed to the high gain (~54 before the onset of significant tunneling current) and low excess noise of InAs APDs. This measurement was corroborated through demonstrations of detecting very weak 1550 nm pulses consisting of <70 photons. In conclusion we have demonstrated the potential of low photon detection using InAs planar APD at the 1550 nm wavelength. It is anticipated that even lower NEPs can be achieved through various set-up and device level optimizations.

References

[1] M. Nada *et al.*, 'High-speed III-V based avalanche photodiodes for optical communications—the forefront and expanding applications', *Appl. Phys. Lett.*, vol. 116, no. 14, p. 140502, Apr. 2020, doi: 10.1063/5.0003573.

[2] Q. Hao, Y. Tao, J. Cao, and Y. Cheng, 'Development of pulsed-laser three-dimensional imaging flash lidar using APD arrays', *Microw. Opt. Technol. Lett.*, vol. 63, no. 10, pp. 2492–2509, Oct. 2021, doi: 10.1002/mop.32978.

[3] J. Hodgkinson and R. P. Tatam, 'Optical gas sensing: a review', *Meas. Sci. Technol.*, vol. 24, no. 1, p. 012004, Jan. 2013, doi: 10.1088/0957-0233/24/1/012004.

[4] R. J. McIntyre, 'Multiplication noise in uniform avalanche diodes', *IEEE Trans. Electron Devices*, vol. ED-13, no. 1, pp. 164–168, Jan. 1966, doi: 10.1109/T-ED.1966.15651.

[5] L. J. J. Tan, J. S. Ng, C. H. Tan, and J. P. R. David, 'Avalanche Noise Characteristics in Submicron InP Diodes', *IEEE J. Quantum Electron.*, vol. 44, no. 4, pp. 378–382, Apr. 2008, doi: 10.1109/jqe.2007.914771.

[6] 'Excelitas Technologies, C30921SH datasheet', 2014.

[7] Y. Cao, T. Blain, J. D. Taylor-Mew, L. Li, J. S. Ng, and C. H. Tan, 'Extremely low excess noise avalanche photodiode with GaAsSb absorption region and AlGaAsSb avalanche region', *Appl. Phys. Lett.*, vol. 122, no. 5, p. 051103, Jan. 2023, doi: 10.1063/5.0139495.

[8] X. Collins *et al.*, 'Low-noise AlGaAsSb avalanche photodiodes for 1550nm light detection', in *Optical Components and Materials XIX*, M. J. Digonnet and S. Jiang, Eds., San Francisco, United States: SPIE, Mar. 2022, p. 16. doi: 10.1117/12.2608842.

[9] J. Abautret, J. P. Perez, A. Evirgen, J. Rothman, A. Cordat, and P. Christol, 'Characterization of midwave infrared InSb avalanche photodiode', *J. Appl. Phys.*, vol. 117, no. 24, p. 244502, Jun. 2015, doi: 10.1063/1.4922977.

[10] X. Sun, J. B. Abshire, J. D. Beck, P. Mitra, K. Reiff, and G. Yang, 'HgCdTe avalanche photodiode detectors for airborne and spaceborne lidar at infrared wavelengths', *Opt. Express*, vol. 25, no. 14, p. 16589, Jul. 2017, doi: 10.1364/OE.25.016589.

[11] X. Sun *et al.*, 'HgCdTe avalanche photodiode array detectors with single photon sensitivity and integrated detector cooler assemblies for space lidar applications', *Opt. Eng.*, vol. 58, no. 06, p. 1, Jun. 2019, doi: 10.1117/1.OE.58.6.067103.

[12] W. Lei, J. Antoszewski, and L. Faraone, 'Progress, challenges, and opportunities for HgCdTe infrared materials and detectors', *Appl. Phys. Rev.*, vol. 2, no. 4, p. 041303, Dec. 2015, doi: 10.1063/1.4936577.

[13] M. A. Coulter, 'Minamata Convention on Mercury', *Int. Leg. Mater.*, vol. 55, no. 3, pp. 582–616, Jun. 2016, doi: 10.5305/intelegamate.55.3.0582.

[14] I. C. Sandall, J. S. Ng, S. Xie, P. J. Ker, and C. H. Tan, 'Temperature dependence of impact ionization in InAs', *Opt. Express*, vol. 21, no. 7, p. 8630, Apr. 2013, doi: 10.1364/oe.21.008630.

[15] C. H. Tan, A. Velichko, L. W. Lim, and J. S. Ng, 'Few-photon detection using InAs avalanche photodiodes', *Opt. Express*, vol. 27, no. 4, p. 5835, Feb. 2019, doi: 10.1364/OE.27.005835.

[16] W. Sun *et al.*, 'High-Gain InAs Avalanche Photodiodes', *IEEE J. Quantum Electron.*, vol. 49, no. 2, pp. 154–161, Feb. 2013, doi: 10.1109/JQE.2012.2233462.

[17] B. S. White *et al.*, 'High-Gain InAs Planar Avalanche Photodiodes', *J. Light. Technol.*, vol. 34, no. 11, pp. 2639–2644, Jun. 2016, doi: 10.1109/JLT.2016.2531278.

[18] A. R. J. Marshall, P. J. Ker, A. Krysa, J. P. R. David, and C. H. Tan, 'High speed InAs electron avalanche photodiodes overcome the conventional gain-bandwidth product limit', *Opt. Express*, vol. 19, no. 23, p. 23341, Nov. 2011, doi: 10.1364/OE.19.023341.

[19] T. Osman, L. W. Lim, J. S. Ng, and C. H. Tan, 'Fabrication of infrared linear arrays of InAs planar avalanche photodiodes', *Opt. Express*, vol. 30, no. 12, p. 21758, Jun. 2022, doi: 10.1364/OE.460017.

[20] J. F. Ziegler, M. D. Ziegler, and J. P. Biersack, 'SRIM – The stopping and range of ions in matter (2010)', *Nucl. Instrum. Methods Phys. Res. Sect. B Beam Interact. Mater. At.*, vol. 268, no. 11–12, pp. 1818–1823, Jun. 2010, doi: 10.1016/j.nimb.2010.02.091.

[21] P. J. Ker, 'Development of high speed low noise InAs electron avalanche photodiodes', PhD Thesis, The University of Sheffield, Department of Electronic and Electrical Engineering, 2012.

[22] L. W. Lim, C. H. Tan, J. S. Ng, J. D. Petticrew, and A. B. Krysa, 'Improved Planar InAs Avalanche Photodiodes With Reduced Dark Current and Increased Responsivity', *J. Light. Technol.*, vol. 37, no. 10, pp. 2375–2379, May 2019, doi: 10.1109/JLT.2019.2905535.